Experimental Reports

(2019)

Activity Report on Neutron Scattering Research: Experimental Reports Vol. 25 (2019)

Published by:
Neutron Science Laboratory,
Institute for Solid State Physics,
University of Tokyo
106-1, Shirakata, Tokai,
Ibaraki 319-1106,
JAPAN

This volume contains experimental reports submitted in the following period of time: 2019/08/01 to 2020/08/31.
Visit our on-line database for updated information.

Structures and Excitations

Magnetism

- Neutron powder diffraction study on the Au-Ga-Tb quasicrystal approximant
  T. J. Sato, A. Ishikawa, S. Yoshida, Chin-Wei Wang, and R. Tamura
  Activity Report on Neutron Scattering Research: Experimental Reports **25** (2020) Report Number: 1955

- Phase diagram of the moving magnetic skyrmion lattice with plastic deformation in MnSi under high electric current
  D. Okuyama, S. Aji, N. Booth, E. Gilbert, M. Bleuel, Q. Ye, A. Kikkawa, Y. Taguchi, Y. Tokura, Y. Nambu, and T. J. Sato
  Activity Report on Neutron Scattering Research: Experimental Reports **25** (2020) Report Number: 1956

- Spin excitations in the skyrmion lattice phase of MnSi1-xGex
  Seno Aji, Daisuke Okuyama, Kazuhiro Nawa, Shinichiro Yano, and Taku J. Sato
  Activity Report on Neutron Scattering Research: Experimental Reports **25** (2020) Report Number: 1959

- Magnon polaron induced longevity of the magnon lifetime
  Y. Nambu
  Activity Report on Neutron Scattering Research: Experimental Reports **25** (2020) Report Number: 1963

- Electric field effect on the magnon dispersion in alpha-Cu2V2O7
  Pharit Piyawongwatthana, Yano Shinichiro, Daisuke Okuyama, Kazuhiro Nawa, Kittiwit Matan, and Taku J Sato
  Activity Report on Neutron Scattering Research: Experimental Reports **25** (2020) Report Number: 1964

Strongly Correlated Electron Systems

- Study of 2D Heavy Fermion Compounds Ce(Te1-xSex)3
  R. Kobayashi, D. Ueta
  Activity Report on Neutron Scattering Research: Experimental Reports **25** (2020) Report Number: 1958

- Magnetic correlation at Wannier point in isosceles-triangular lattice Ising magnet CoNb2O6
  S. Mitsuda, Y. Shimoda
  Activity Report on Neutron Scattering Research: Experimental Reports **25** (2020) Report Number: 1961

Glasses and Liquids

- Dynamics of super-high entropy liquids alkylated perfluorobenzenes
  O. Yamamuro, M. Nirei, H. Akiba, T. Nakanishi, M. Tyagi, M. Wolf
  Activity Report on Neutron Scattering Research: Experimental Reports **25** (2020) Report Number: 1966

Biology

- Visualization of domain motion of tri-ubiquitin through segment deuteration and small-angle

neutron scattering
Rintaro Inoue and Masaaki Sugiyama
Activity Report on Neutron Scattering Research: Experimental Reports **25** (2020) Report Number: 1940

Soft Matters

- Effect of a model scramblase peptide on viscoelastic properties of phspholipid bilayers
  Hiroyuki Nakao
  Activity Report on Neutron Scattering Research: Experimental Reports **25** (2020) Report Number: 1954

Structures and Excitations

Crystal structure analysis of high temperature neutron diffraction data of Zn containing oxide-ion conductors

Kotaro Fujii, Hiroaki Tejima, Wenrui Zhang, Yuta Yasui, Masatomo Yashima
Tokyo Institute of Technology

Oxide-ion conductors, which include pure ionic conductors and mixed oxide-ion and electronic conductors, attract significant interest because of their varied uses in oxygen separation membranes and cathodes for solid-oxide fuel cells (SOFCs). The oxide-ion conductivity is strongly dependent on the crystal structure. At present, several structures, such as fluorites, perovskites, K_2NiF_4, mellilites, and apatites, are known to show high oxide-ion conductivities. For further developments, it is necessary to find new structure families of oxide-ion conductors. According to such background, we are exploring new structure family of oxide-ion conductors. For example, we previously discovered new structural families of oxide-ion conductors $BaNdInO_4$, $Ca_{0.8}Y_{2.4}Sn_{0.8}O_6$, $Ca_3Ga_4O_9$, and $BaHo_2ZnO_5$. Recently, we found a new structure family of oxide-ion conductor, which containing zinc (Zn) as an essential element. In order to understand the mechanism of oxide-ion conduction, it is necessary to precisely determine the crystal structure (particularly position, occupancy factor, and anisotropic displacement parameters of oxygens) at high-temperature because oxide-ion conductors are generally used at high-temperature. In the present study, we investigated the crystal structure of this new Zn-containing oxide-ion conductor at high temperature using high resolution neutron powder diffractometer Echidna installed at the research reactor OPAL, ACNS, ANSTO. The material was prepared by the solid-state reaction. Sintered pellets of the reaction products were introduced into a vanadium can and used for the neutron diffraction experiment. The measurements were carried out from room temperature to high temperature (1100 °C). Each measurement took about 3 hours. The reflection positions were shifted toward low angle by heating, which suggests the lattice parameters were expand by heating (see figure). Structural analyses are now undergoing by Rietveld method using the program Z-code. Our structure analysis reveal the present material contains positional disorder for the oxygen atoms, which has not been reported in the previous studies. This result indicate the neutron diffraction study is very important to lead the precise and correct atomic position and displacement parameters of oxygen atoms.

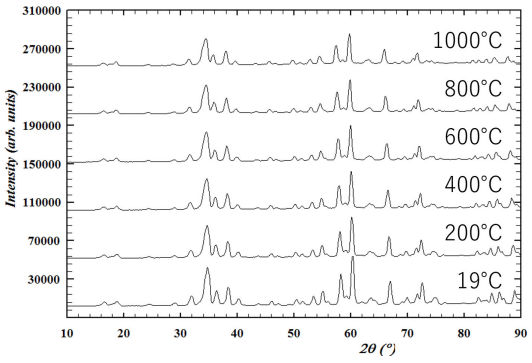

Fig. 1.

Structure analysis of novel oxide-ion conductors from neutron powder diffraction data

K. Fujii[A], Y. Yasui[A], H. Tejima[A], T. Murakami[A], M. Yashima[A]
[A] *School of Science, Tokyo Institute of Technology*

Oxide-ion conductors, which include pure ionic conductors and mixed oxide-ion and electronic conductors, attract significant interest because of their varied uses in oxygen separation membranes and cathodes for solid-oxide fuel cells (SOFCs). The oxide-ion conductivity is strongly dependent on the crystal structure. At present, several structures, such as fluorites, perovskites, K_2NiF_4, mellilites, and apatites, are known to show high oxide-ion conductivities. For further developments, it is necessary to find new structure families of oxide-ion conductors. According to such background, we are exploring new structure family of oxide-ion conductors. For example, we previously discovered new structural families of oxide-ion conductors $BaNdInO_4$,[1] $Ca_{0.8}Y_{2.4}Sn_{0.8}O_6$,[2] $BaHo_2ZnO_5$, [3] and $Ca_3Ga_4O_9$. [4] Recently, we found several new oxide-ion conductors. In order to understand the mechanism of oxide-ion conduction, it is necessary to precisely determine the crystal structure (particularly position, occupancy factor, and anisotropic displacement parameters of oxygens) at high-temperature because oxide-ion conductors are generally used at high-temperature. In the present study, we investigated the crystal structure of these new oxide-ion conductors using high resolution neutron powder diffractometer Echidna installed at the research reactor OPAL, ACNS, ANSTO.

Constant-wavelength neutron powder diffraction data of the prepared samples were measured at 24°C and high temperature (200, 400, 600, and 800 °C). The measurement conditions were wavelength: 1.622652(14) Å step interval: 0.125° in 2θ / step. For the high-temperature measurements, the samples were heated with a vacuum furnace at 10^{-4} Pa during the neutron-diffraction measurements.

We are now analyzing the neutron diffraction data by Rietveld method. Fig. 1(a) shows the preliminary obtained Rietveld plot of the new oxide-ion conductor containing Ba, Ca, Mn, and O. Basically good fitting was obtained but still containing bad fitting for some reflections. To improve the fitting, we are now trying to make better structure model for this compound.

Fig. 1(b) shows neutron diffraction patterns of Ba-Ho-Zn containing new oxide-ion conductor taken at 24, 200, 400, 600, and 800°C. With increasing temperature, lattice volume expansions were observed as the peak position shifts toward lower angle. The data analysis is in progress.

[1] K. Fujii et al., Chem. Mater. 26, 2488 (2014).
[2] R. Inoue et al., Dalton Trans. 47, 7515 (2018).
[3] K. Nakamura et al., J. Ceram. Soc. JPN. 126, 929 (2018).
[4] Y. Yasui et al., Inorg. Chem. 58, 9560 (2019).

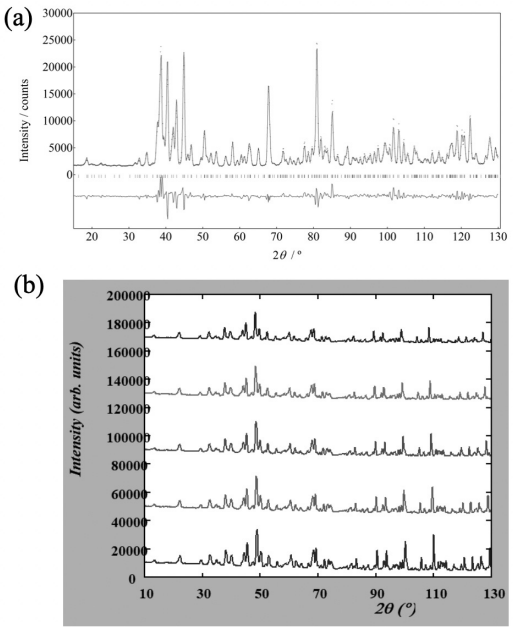

Fig. 1. (a) Rietveld plot of the new oxide-ion conductor containing Ba, Ca, Mn, and O. (b) Neutron diffraction patterns of Ba-Ho-Zn containing new oxide-ion conductor taken at 24, 200, 400, 600, and 800°C (from bottom to top).

Dynamics of hydrogen atoms in PdPt nanoparticles

O. Yamamuro[A], H. Akiba[A], H. Kobayashi[B], H. Kitagawa[B], N. De Souza[C], R. Mole[C]
[A]*ISSP-NSL, Univ. of Tokyo,* [B]*Kyoto Univ.,* [C]*ACNS, ANSTO*

The nanometer-sized metals attract much attention since their physical and chemical properties are substantially different from those of bulk metals. Kobayashi et al. found that the phase-separated nanoparticles of Pd-core and Pt-shell are mixed to be solid solution alloy by repeating hydrogen absorption/desorption processes at 373 K [1]. Our neutron powder diffraction (NPD) measurements for solid solution Pd0.8Pt0.2D0.36 nanoparticles revealed that D atoms are located at the interstitial octahedral (O) and tetrahedral (T) sites of an fcc lattice, as schematically shown in the inset of Fig. 1 [2]. Interestingly, 47% of D atoms occupy the T sites even at 300 K, which is larger than that for $PdD_{0.36}$ nanoparticles (31%). This means that the hydrogen absorption sites (T-sites) are more stabilized by the insertion of Pt atoms, although single Pt metal does not absorb hydrogen. In this study, we have investigated the diffusion dynamics of hydrogen atoms in solid solution $Pd_{0.8}Pt_{0.2}$ nanoparticles by means of quasielastic neutron scattering (QENS).

The mean diameter of $Pd_{0.8}Pt_{0.2}$ nanoparticles was determined to be 5.0 nm from TEM images. The nanoparticles are covered by protection polymer, polyvinylpyrrolidone (PVP), to avoid the adhesion between the nanoparticles. The total amount of sample with PVP was 766 mg. The hydrogenation was carried out at 100 kPa and 21°C for 1 day. The hydrogen concentration ($x = 0.47$) was determined from the reduction in H_2 pressure of the gas handling system. The QENS experiments were performed on Pelican and Emu spectrometers at ACNS, ANSTO. Using these instruments, we have investigated the relaxation phenomena in time range from 1 ps to 5 ns.

Figure 1 shows the Arrhenius plot of the relaxation times (τ) for $Pd_{0.8}Pt_{0.2}H_{0.47}$ nanoparticles obtained by Emu (▲) and Pelican (●). We also plot the data for $PdH_{0.47}$ nanoparticles (▽) obtained in our previous QENS experiments [3]. There are two relaxation processes in both $Pd_{0.8}Pt_{0.2}H_{0.47}$ and $PdH_{0.47}$ nanoparticles. From our previous results [2,3], we assign the slow and fast relaxation processes to the hydrogen motions in the interior and subsurface regions of nanoparticle, respectively. In the slow relaxation process, the τ and the activation energy of $Pd_{0.8}Pt_{0.2}H_{0.47}$ nanoparticles are smaller than those for $PdH_{0.47}$ nanoparticles. Interestingly, the fast relaxation time for $Pd_{0.8}Pt_{0.2}H_{0.47}$ nanoparticles is almost temperature independent below 250 K, suggesting tunneling processes. Thus, the substitution of Pt atoms in a Pd fcc lattice deforms the potential energy surfaces and enhances the diffusion of hydrogen atoms.

[1] H. Kobayashi et al., JACS 132, 5576 (2010).
[2] H. Akiba et al., JPCC 123, 9471 (2019).
[3] M. Kofu et al., PRB 94, 064303 (2016)

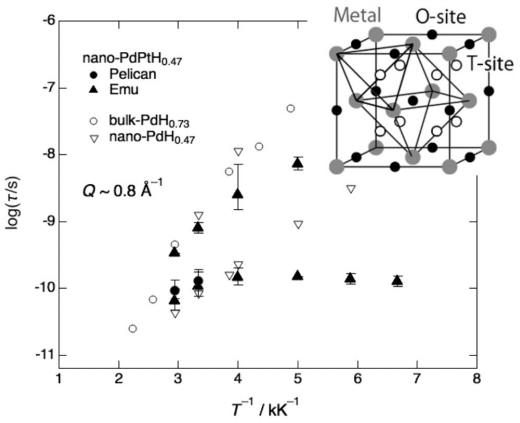

Fig. 1. Arrhenius plot of the relaxation times for $Pd_{0.8}Pt_{0.2}H_{0.47}$ and $PdH_{0.47}$ nanoparticles.

Magnetism

Neutron diffraction study on structural and magnetic properties of the tetragonal Mn3+xGe1-x

H. Okada(A), Y. Nambu(B), M. Avdeev(C,D)
(A)Tohoku Gakuin Univ. (B)IMR, Tohoku Univ. (C)ANSTO (D)Univ. Sydney

Ferrimagnetic Mn3Ga and Mn3Ge with a tetragonal structure are expected to be candidates for novel spintronics and permanent magnet materials [1]. The compounds undergo a structural phase transition accompanied by a magnetic transition from the ferrimagnetic tetragonal phase to a paramagnetic hexagonal high temperature phase. It is known that the offstoichiometric composition is required to obtain the single phase of the tetragonal phase. Recently, we have found that thermal stability of the tetragonal phase in Mn3Ge is expanded by introducing excess Mn. Furthermore, as the result of the enhancement on the thermal stability, we observed that an intrinsic magnetic transition from ferrimagnetic to paramagnetic phases in the tetragonal phase occurs at 860 K. Although the magnetic transition temperature is robust against the introduction of the excess Mn, the magnetization decreases with increasing Mn content. These results clearly indicate that the excess Mn strongly affects the structural and magnetic properties of the tetragonal manganese-germanium compound. A previous report of neutron diffraction experiments suggests that the excess Mn is located at the Ge site [2]. However, the magnitude of magnetic moment is estimated to be 4 - 7 Bohr magneton, which is too large value for magnetic moment. The results obtained from accurate measurement and analysis would lead to further experimental and theoretical investigation and understanding of correlations between the electronic properties and the structural and magnetic properties. In this study, to directly observe the structural phase transition, we have performed neutron diffraction experiments for Mn3+xGe1-x at ECHIDNA in Australian Nuclear Science and Technology Organisation. As shown in the Figure, neutron diffraction pattern of Mn3.03Ge0.97 clearly changes in the vicinity of 858 K, indicating that the tetragonal D022 structure transforms to the hexagonal D019 structure. In case of Mn3.09Ge0.91, the structural phase transition occurs in the vicinity of 928 K, which is higher temperature than that in Mn3.03Ge0.97. These results directly prove that thermal stability of D022 structure in Mn-Ge is expanded by introducing small amount of excess Mn.

[1] B. Balke et al, Appl. Phys. Lett. 90, 152504, 2007.
[2] N. Yamada et al., J. Phys. Soc. Jpn 59 273, 1990.

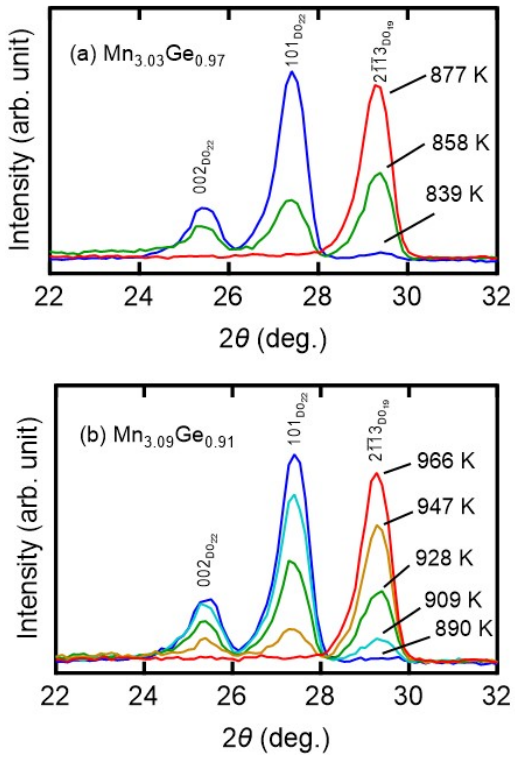

Fig. 1. Neutron diffraction patterns of (a)Mn3.03Ge0.97 and (b)Mn3.09Ge0.91

Crystalline electric field level scheme of the $CeTe_3$

D. Ueta[A], R. Kobayashi[B], S. Yano[C], Y. Okada[A]
OIST[A], University of The Ryukyus[B], NSRRC[C]

What is the ground state of this system when rare-earth atoms, the $4f$-electrons which capture partly itinerant characteristics, occupy a geometrically frustrated site? This fundamental question in condensed matter physics has attracted considerable attention from scientists. However, the experimental elucidation of this question is difficult because there are no samples that satisfy such a situation. In general, the $4f$-electron has large and anisotropic angular momentum and inhibits the realization of an Ising-like structure, which is required for a spin-frustrated system.

RTe_3 (R: rare-earth elements) is composed of a square net Te layer with high mobility and a blocking layer with R-originated $4f$-electrons. A particularly interesting case is R = Ce, since the f-electron exists closer to Fermi energy E_F. According to previous research, the electronic specific coefficient of $CeTe_3$ is larger than that of the La system, suggesting that f-electrons are itinerant. On the other hand, in the isostructural $CeTe_2Se$ in which the doped Se atoms enter the blocking layer selectively, there are no dramatic changes in the magnetic transition temperature towards the QCP. However, from the magnetization measurements of the previous study, in the magnetic ordered state the magnetic moment of the Ce atom lies in the ac-plane (in-plane) on $CeTe_3$ but along the b-axis (out of plane) on $CeTe_2Se$. These results sugget that the ground state is qualitatively different due to the influence of the CEF effect by anion doping.

In order to determine the crystalline electric field (CEF) level scheme in $CeTe_3$, we performed inelastic neutron scattering (INS) experiments using SIKA at the Australian Nuclear Science and Technology Organisation. A single crystalline sample of $CeTe_3$ was grown by a flux method in the Okinawa Institute of Science and Technology Graduate University. Many single crystalline samples totaling about 20 g were enclosed in a copper cell and cooled to 2.7 K.

We have succeeded in observing clear CEF excitations at approximately 10 and 22 meV as shown in Fig. 1(a). Furthermore, we also observed an additional peak at around 0.6 meV due to spin-wave excitation, and this excitation vanishes above the transition temperature (T_{N1} = 3 K) as shown in Fig. 1(b). From previous studies of the magnetic susceptibility, a CEF level scheme with a ground state of $\Gamma_7^{(2)}$ was suggested. These CEF parameters give rise to energy-level splitting from the ground state of 11.2 and 19.8 meV, which are roughly consistent with our INS measurements. However, from an analysis of INS and magnetic susceptibility data with a CEF model calculation, we found that the ground state of $CeTe_3$ is $\Gamma_7^{(1)}$.

Travel expenses were supported by the General User Program for Neutron Scattering Experiments, the Institute for Solid State Physics, The University of Tokyo (proposal no. 19902), and JRR-3 of the Japan Atomic Energy Agency, Tokai, Japan.

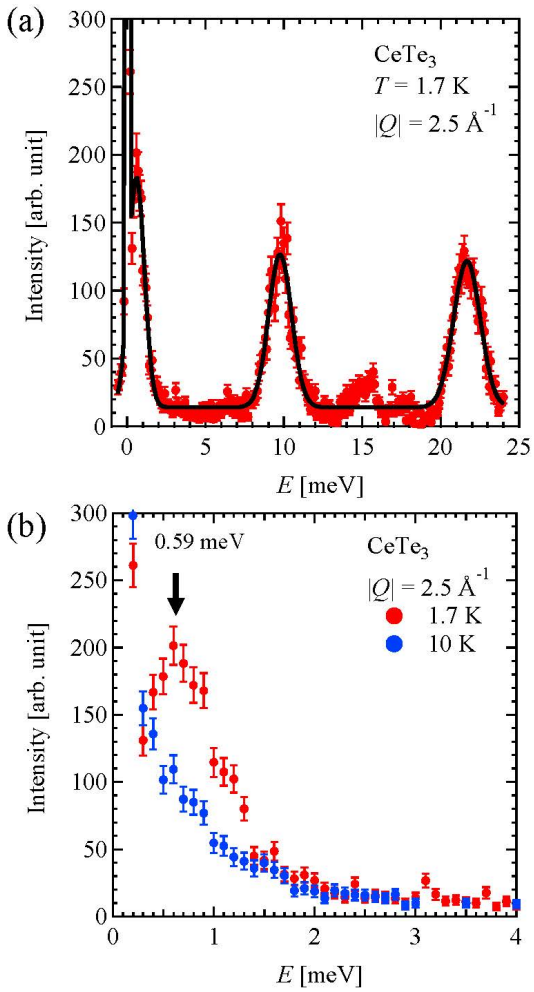

Fig. 1. Inelastic neutron scattering spectra of $CeTe_3$.

Field-induced magnetic order of magnetoplumbite-type cobalt oxide SrCo12O19

Shinichiro Asai, Hodaka Kikuchi, Yuma Iwasaki, Takatsugu Masuda
ISSP, the University of Tokyo

Various physical properties of cobalt oxides have been intensively investigated, which comes from the variety of the electronic states for Co ions. 2+, 3+, and 4+ are stable for the valence of Co ions in oxides. Additionally, the Co3+ ions surrounded by oxygen ions octahedrally can take two different electronic configurations, high-spin state (S = 2) and low-spin state (S = 0).

SrCo12O19 has the magnetoplumbite-type crystal structure as shown in Fig. 1(a) [1]. It consists of the alternate stacking of the SrCo6O11-type blocks and Co3O4-type blocks. From the bond-valence sums, the valences of the Co ions in Co(3) and Co(4) sites are predicted to be 3+ and 2+, respectively [1]. On analogy of SrCo6O11 [2], the Ising-like character is expected for the spins of the Co(3) ions. The uniaxial colossal magnetoresistance was observed in the insulating phase [3]. Ishiwata et al. suggests that the origin of the magnetoresistance is that the charge order in the conduction paths is destabilized by the applied field, and that the uniaxial character of the magnetoresistance is related to the Ising-spins located on Co(3) sites [3]. The magnetic susceptibility has a sharp increase in the case that the magnetic field is perpendicular to the crystallographic c axis at 80 K, which suggests the magnetic long-range order [3].We performed a neutron diffraction experiment at powder diffractometer WOMBAT installed in ANSTO to identify the magnetic state of SrCo12O19. Magnetic peaks indicating the magnetic propagation vector to be (0, 0, 0) were observed below 80 K. The antiferromagnetic order where the ordered moments are located on Co(4) sites reproduces the magnetic peak profile. The interesting point is that the Co(3) ions still have no ordered moments at zero field. In SrCo6O11, the Ising spins are not ordered at zero field, and the ferrimagnetic structure is realized as the field-induced state [4]. The magnetization-field curve of SrCo12O19 at 2 K has the metamagnetic-like anomaly similar with that of SrCo6O11, which indicates that the field-induced states are realized.

Neutron diffraction experiment was performed on High-Intensity Powder Diffractometer WOMBAT installed at ANSTO. 0.9 g of the polycrystalline sample was used. We used the magnet for applying magnetic field. We measured the neutron diffraction patterns at 2 K under the magnetic field of 0, 2, 4, 6, 7, 8, and 9 T. We further measured the pattern at 100 K without the magnetic field in order to obtain the nuclear peak profile for the subtraction.

Neutron diffraction profiles at 2 K under several magnetic fields are shown in Fig. 1(b). The profile at 100 K under zero field is subtracted from these profiles as the background intensities. Five magnetic peaks indexed by (004), (101), (103), (104), (105) were observed at zero field. In addition, the (102) magnetic peak was induced by the magnetic field. Its intensity increases with increasing magnetic field up to 9 T. Meanwhile, the intensity of the (101) peaks decreases a little with increasing magnetic field. It indicates that new magnetic phase with the propagation vector of (0, 0, 0) is induced. The magnetic structure analysis is in progress.

[1] S. Ishiwata et al., J. Solid State Chem. 181, 1273 (2008). [2] S. Ishiwata et al., Phys. Rev. Lett. 98, 217201 (2007). [3] S. Ishiwata et al., Phys. Rev. B 83, 020401 (2011). [4]. T. Saito et al., J. Mag. Mag. Mater. 310, 1584 (2007).

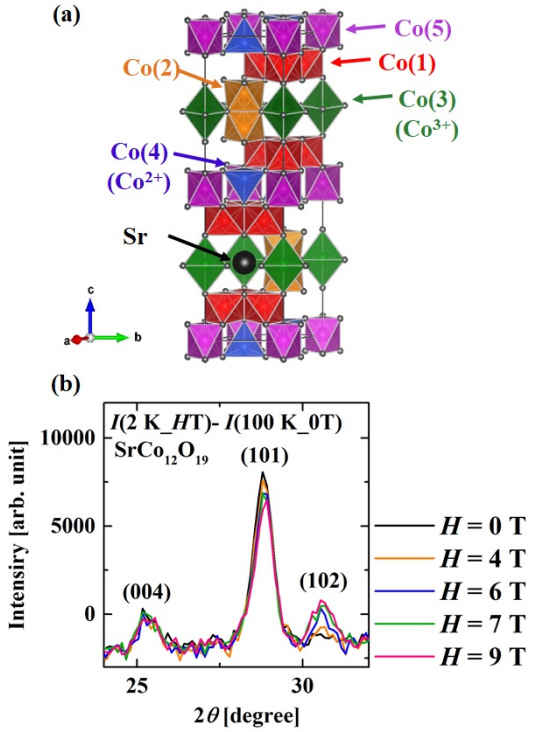

Fig. 1. (a) Crystal structure of SrCo12O19. (b) Neutron diffraction profiles at 2 K under several magnetic fields. The profile at 100 K under zero field is subtracted from the profiles as the background intensities.

Neutron powder diffraction study on the Au-Ga-Tb quasicrystal approximant

T. J. Sato, A. Ishikawa[1], S. Yoshida[1], Chin-Wei Wang[2,3], and R. Tamura[1]
IMRAM Tohoku University, [1]Tokyo University of Science, [2]ANSTO, [3]NSRRC

Quasicrystal is a substance with long-range quasiperiodic atomic arrangement, nonetheless, with the rotational symmetry that is prohibited in the periodic crystals, such as the five-fold symmetry. The quasicrystal is, therefore, different from periodic crystals and random glasses, and now is regarded as the third form of solids. There is a class of crystals, called "approximants", in which the high-symmetry (such as icosahedral) atomic clusters, identical to those in the quasicrystals, form periodic array, and thus being approximation of the quasicrystalline structure. Recently, for the first time we have determined magnetic structure of the antiferromagnetic 1/1 Au-Al-Tb approximant using ECHIDNA [1], which turns out to be a very intriguing non-collinear and non-coplanar whirling order. We also have performed single crystal neutron diffraction on the macroscopically ferromagnetic quasicrystal approximant Au-Si-Tb [2]. Together with the crystalline-electric-field anisotropy estimated from inelastic neutron scattering spectra, we also proposed nontrivial non-collinear and noncoplanar magnetic structure quite similar to that observed in the Au-Al-Tb. In this work, to accumulate knowledge on the magnetic ordering in the quasicrystal approximants, powder neutron diffraction was performed on the Au-Ga-Tb 1/1 approximant.

A polycrystalline alloy of the Au-Ga-Tb 1/1 approximant was prepared by arc melting with high purity Au, Ga and Tb elements with proper heat treatment to obtain single phase specimen. The neutron powder diffraction experiment has been performed using the high-resolution powder diffractometer ECHIDNA installed at the OPAL reactor, Australian Nuclear Science and Technology Organisation [3]. For most of the magnetic diffraction measurement, neutrons with $\lambda = 2.4395$ Å was selected using the Ge 311 reflections, whereas for the structure analysis, to obtain reflections in a wide Q-range, we select $\lambda = 1.622$ Å using the Ge 335 reflections. The sample was set in the ϕ6 mm vanadium sample can, and then set to the cold head of the closed cycle ^{4}He refrigerator with the base temperature 3.5 K.

Figure shows the overall diffractograms at the base temperature ($\simeq$ 3.5 K) and the paramagnetic temperature $T = 20$ K. One can clearly see the development of sharp magnetic reflections at the base temperature. They are the clear indication of magnetic long-range order in this 1/1 approximant. The magnetic structure analysis using the representation analysis is now under way.

References: [1] T. J. Sato, A. Ishikawa, A. Sakurai, M. Hattori, M. Avdeev and R. Tamura, Phys. Rev. B 100, 054417 (2019); [2] T. Hiroto, T. J. Sato, H. Cao, T. Hawai, T. Yokoo, S. Itoh, and R. Tamura, J. Phys.: Condens. Matter (in press); [3] M. Avdeev and J. R. Hester, J. Appl. Crystallogr. 51, 1597 (2018).

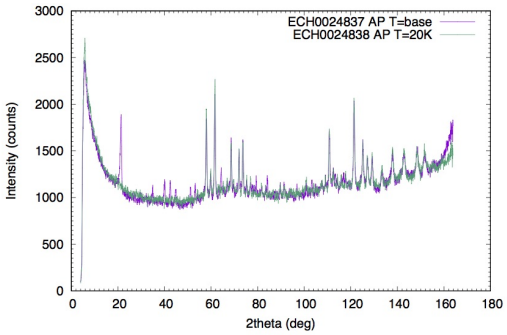

Fig. 1. Neutron diffraction patterns obtained in at the base temperature ($\simeq$ 3.5 K) and the paramagnetic temperature $T = 20$ K at ECHIDNA.

Phase diagram of the moving magnetic skyrmion lattice with plastic deformation in MnSi under high electric current

D. Okuyama[1], S. Aji[1], N. Booth[2], E. Gilbert[2], M. Bleuel[3], Q. Ye[3], A. Kikkawa[4], Y. Taguchi[4], Y. Tokura[4,5], Y. Nambu[6], and T. J. Sato[1]

[1]*IMRAM, Tohoku Univ.*, [2]*ANSTO*, [3]*NCNR, NIST*, [4]*RIKEN-CEMS*, [5]*Univ. of Tokyo*, [6]*IMR, Tohoku Univ.*

A magnetic skyrmion is formed by a swirling spin texture. Such a swirling structure is characterized by a discrete topological number, called as skyrmion number. In the prototypical chiral magnet MnSi, magnetic skyrmions condense into triangular-lattice, observed as six-fold magnetic Bragg reflections in small-angle neutron scattering (SANS) [1]. In metallic skyrmion compounds, there is important characteristic, i.e., its surprisingly large coupling with the electric current flow. The electric current density required to realize the skyrmion lattice motion in chiral magnet MnSi is considerably small as $j_t \sim 1$ MA/m^2 [2]. Hence, the magnetic skyrmion in MnSi attracts growing attention recently, and is under intense scrutiny for elucidating its dynamical behavior under electric current. We performed SANS experiment in chiral magnet MnSi with suppressing thermal gradient as much as experimentally achievable. SANS experiments were carried out at NG7 in NIST and at QUOKKA in ANSTO. A direct electric current or an alternative electric current with square wave form was applied along the [0 0 1] direction. The sample mount was attached to the sample stick, and was installed in the horizontal field magnet with the magnetic field applied along [1 -1 0] parallel to the incident neutron beam. We observed the six-hold magnetic skyrmion reflections in the skyrmion phase under the electric current density $j = 0$. In the previous experiments, we found a spatially inhomogeneous counterrotating behavior of the magnetic skyrmion reflections measured at left-edge and right-edge above the threshold current density j_t [3]. The rotation direction of the magnetic skyrmion reflections can be inverted by the inversion of the electric current direction. In this time, we performed SANS experiment on the left-edge and right-edge of the MnSi sample under an alternative electric current flow to investigate a rotational dynamics of the magnetic skyrmion lattice. The size of the neutron illumination area is approximately 0.2 mm (width) $\times$ 1.0 mm (height). At the alternative electric current desnsity $j_{ac} > j_t$, the rotational motion of the magnetic skyrmion reflections follows an obvious alternative electric current frequency dependence. By the fitting of a naive Debye relaxation type function, we estimated the relaxation time t_r. In the frequency region of the alternative electric current below $1/t_r$, the rotational direction of the magnetic skyrmion reflections follows the inversion of the alternative electric current direction. In stark contrast, the magnetic skyrmion reflections do not respond when the frequency of the alternative electric current is higher than $1/t_r$. These results indicate that magnetic skyrmion lattices under current flow experience significant friction near the sample edges, and the rotational motion of the magnetic skyrmion reflections shows Debye type relaxation under the alternative electric current. Such a dynamics information of the magnetic skyrmion lattice being important factors that must be considered for the anticipated skyrmion-based applications in chiral magnets at the nanoscale. In summary, we have used SANS to study skyrmion-lattice motion in chiral magnet MnSi under an alternative electric current flow. The frequency dependence of the rotation motion of the magnetic skyrmion reflections was measured under an alternative electric current

density $j_{ac} > j_t \sim 1\,\mathrm{MA/m^2}$.

Reference: [1] S. Muhlbauer, B. Binz, F. Jonietz, C. Pfleiderer, A. Rosch, A. Neubauer, R. Georgii, and P. Boni, Science 323, 915 (2009). [2] F. Jonietz, S. Muhlbauer, C. Pfleiderer, A. Neubauer, W. Munzer, A. Bauer, T. Adams, R. Georgii, P. Boni, R. A. Duine, K. Everschor, M. Garst, and A. Rosch, Science 330, 1648 (2010). [3] D. Okuyama, M. Bleuel, J.S. White, Q. Ye, J. Krzywon, G. Nagy, Z.Q. Im, I. Zivkovic, M. Bartkowiak, H.M. Ronnow, S. Hoshino, J. Iwasaki, N. Nagaosa, A. Kikkawa, Y. Taguchi, Y. Tokura, D. Higashi, J.D. Reim, Y. Nambu, and T.J. Sato, Commun. Phys. 2, 79 (2019).

Spin excitations in the skyrmion lattice phase of $MnSi_{1-x}Ge_x$

Seno Aji[A], Daisuke Okuyama[A], Kazuhiro Nawa[A], Shinichiro Yano[B], and Taku J. Sato[A]
[A]*IMRAM, Tohoku University,* [B]*NSRRC*

MnSi is the chiral magnetic compound and attracts renewed interest because of the discovery of the skyrmion-lattice structure under finite magnetic field [1]. The magnetic skyrmion is a topological spin texture made of swirling magnetic moments. Recently, the spin excitations so called 'magnon' in such spin texture was studied theoretically and was found that topological nature of skyrmion will give non-trivial topological number (Chern number) for each magnon bands, resulting in the formation of the topological magnon band [2]. Here, we study such a topological magnon bands experimentally in MnSi and Ge-doped MnSi. Single crystal samples of MnSi (18 grams) and $MnSi_{0.98}Ge_{0.02}$ (15.5 grams) were used in the experiments. The single crystals were grown using Bridgmann furnace with temperature and transport speed of 1573 K and 4 mm/hour, respectively. We performed elastic and inelastic neutron experiments using SIKA spectrometer in ANSTO. For the neutron experiment, the samples were mounted in the aluminum plate and aligned with 110 and 001 in the scattering plane. This configuration will set 110 as the magnetic field direction. The samples were placed in the cryostat equipped with a vertical superconducting magnet. Pyrolytic graphite PG 002 reflections were used for monochromator and analyzer. The collimation settings were Open-20'-20'-60' with vertically focusing monochrome tor mode. The final neutron energy was fixed to 2.75 meV.

The magnetic modulation vector Q of MnSi and $MnSi_{0.98}Ge_{0.02}$ were obtained as 0.035 and 0.046 Å from elastic scattering measurement. The inelastic scattering experiment was carried out by setting the temperature of 28.6 K (MnSi) and 30.5 K ($MnSi_{0.98}Ge_{0.02}$) and magnetic field of 0.2 T for both samples judging from the optimum intensity of the magnetic field scan in the skyrmion lattice phase by the elastic experiment. The low-energy magnetic excitation modes were observed at several Q points. Fig. 1(a) is a representative result of low-energy magnetic excitations observed at M point for both samples. Excitation spectra for $MnSi_{0.98}Ge_{0.02}$ are weaker and broader. Excitation spectra also get weaker at higher Q-positions (Fig 1(b)). We confirmed that this excitation is intrinsic in the skyrmion-lattice phase, by comparing it to the excitation spectra both in the fully-polarized and helical phases.

[1] S. Muhlbauer et al., Science 323, 915 (2009).

[2] A Roldan-Molina et al., New J. Phys. 18, 045015 (2016).

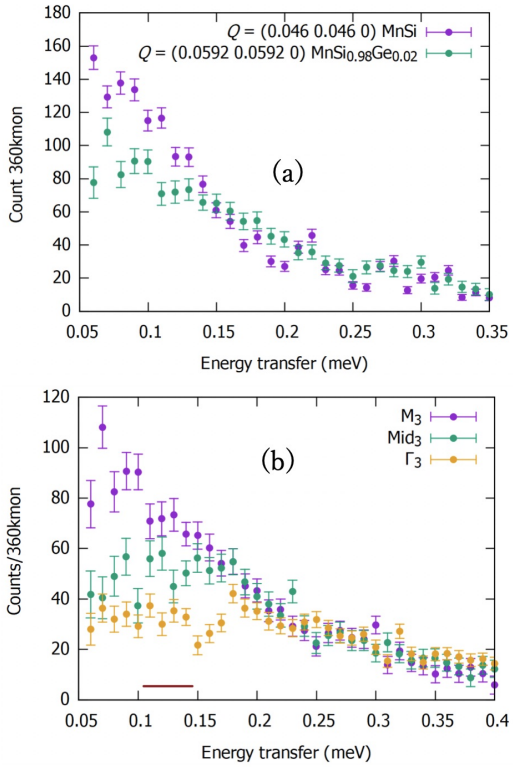

Fig. 1. (a) The observed low-energy magnetic excitations at M point for MnSi and $MnSi_{0.98}Ge_{0.02}$, and (b) Q-position dependence of inelastic spectra for $MnSi_{0.98}Ge_{0.02}$.

Magnetic correlation at Wannier point in isosceles-triangular lattice Ising magnet $CoNb_2O_6$

S. Mitsuda[A], Y. Shimoda[A]
[A] *Department of Physics, Faculty of Science, Tokyo University of Science*

Recently, we have studied an isosceles triangular lattice Ising magnet $CoNb_2O_6$ along the context that if the ratio of exchange interactions defined as $\gamma = J_1$ (along the base direction) $/J_2$ (along the equilateral direction) can be controlled via anisotropic deformation of isosceles triangular lattice (ITL) by uniaxial pressure, variety of interesting magnetic features intrinsic to γ would be observed [1]. Actually along this context, we succeeded in crossing the Wannier point ($\gamma = 1$) by applying the c axis-uniaxial pressure $p \parallel c$ up to 1 GPa, as is in the experimental reports of No.1802 and No.1841. As a continuation of the proposal, using the two-axis diffractometer E4 installed at the Berlin Neutron Scattering Center in the Helmholtz Centre Berlin for Materials and Energy, we tried to provide access to Wannier point by applying the b axis uniaxial pressure $p \parallel b$ up to 1GPa, because almost flat diffraction profile in $(0k0)$ scan can be seen at $p \parallel b \sim 0.6$ GPa ($\gamma \sim 1$) and suggests good "spot" as is in the experimental reports of No.1913.

As shown in Fig.1, switching from AF-II magnetic ordering to AF-I magnetic ordering at $p \parallel b \sim 0.6$ GPa is not sharp but rather broad in contrast to that at $p \parallel c$ ~0.8 GPa. At the same time, with increasing the b axis uniaxial pressure $p \parallel b$, AF-II-2(+) magnetic ordering start to appear, and shows its maximum at $p \parallel b \sim 350$ MPa, and decreases in synchronized with AF-II magnetic ordering. Taking into account that AF-II-2(+) magnetic structure with doubling along both the a and the b directions is stabilized under unequal coupling constants J_2 along equilateral direction of ITL, unfortunately, the b axis-uniaxial pressure produced by our transverse-pressure device in present measurement seems to be in-homogenous and to deviate from the b-axis direction so as to break the equality in J_2 along equilateral direction of ITL.

[1] S. Kobayashi et al., Phys. Rev. B 90, 060412(R).

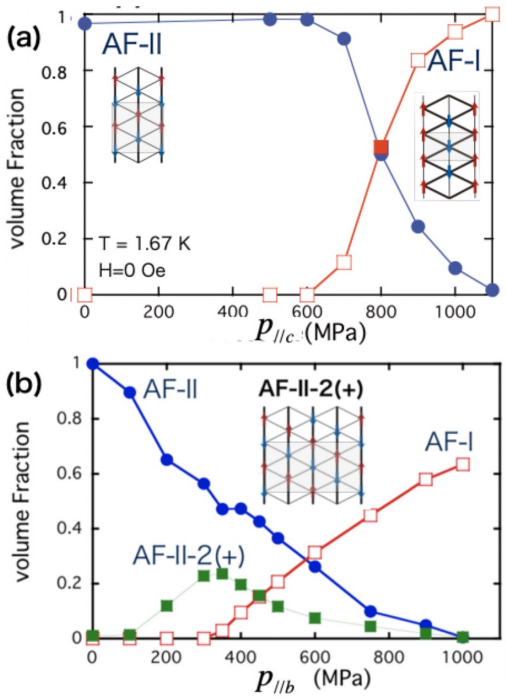

Fig. 1. (a) The c-axis pressure dependence of volume fraction of AF-I, AF-II magnetic orderings, (b) the b-axis pressure dependence of volume fraction of AF-I, AF-II and AF-II-2(+) magnetic orderings.

Magnon polaron induced longevity of the magnon lifetime

Y. Nambu[A]
[A]*Institute for Materials Research, Tohoku University*

Magnon (spin wave) and phonon (sound wave) are collective excitations of ordered magnetic moments and lattice vibrations, respectively. When the sound wave travels in a magnet, local distortions exert torques on the magnetic order through the magneto-elastic coupling. Propagating magnons affect the lattice dynamics, vice versa. The coupling between spin and sound waves has thus been intensively studied in the last half-century. Nowadays they are known to hybridize at (anti-)crossing points of their dispersion relations [1], forming coherently mixed quasiparticles "magnon polarons," when the lifetime of quasiparticles is well-defined compared to the magnitude of the anti-crossing gap.

Although hybridized magnon-phonon states (or magnon polaron) were predicted a long time ago [1], their effects on magnon spin transport have been elucidated quite recently in yttrium iron garnet ($Y_3Fe_5O_{12}$: YIG) by the spin Seebeck effect (SSE) observations. The measurement was made through the generation of a spin current with a temperature gradient in YIG [2,3]. Reference [2] showed that the hybridization of magnon and phonon could lead to resonant enhancement of the SSE signal. The enhancement emerges by the magnetic field application, where the acoustic phonon dispersion becomes tangential to the magnon one. The result in Ref. [2] is indeed well explained in terms of the longevity of phonon than magnon; owing to the phononic constituent of magnon polarons, the condition makes magnon-polaron lifetime longer than pure magnon lifetime, leading to the enhanced spin current by the hybridization [2]. This lifetime enhancement of magnon through magnon polaron hybridization is indeed observed by our recent neutron scattering experiment. Here we would like to clarify such an enhancement of the magnon lifetime using polarized neutrons.

In the polarized neutron scattering experiment on the cold neutron triple-axis spectrometer V2 FLEXX at Helmholtz Zentrum Berlin, Germany, we used a single crystal (mass $\sim$ 8 g) of YIG with a horizontal scattering zone $[HHL]$. We chose the P_x polarization (neutron polarization parallel to the momentum transfer) and recorded all the four channels such as σ^{++}, σ^{+-}, σ^{-+} and σ^{--} with applying horizontal magnetic fields. First, the (220) Bragg reflection was confirmed by the diffraction mode. Phonon and magnon dispersion relations were already known from our previous experiment [4], we then planned to collect energy scans at several displaced positions from (220) for both longitudinal and transverse directions. All the measurements were performed at temperature 100 K, and as a function of fields up to 3 T. We successfully observed magnon lifetime enhancement at 2.5 T that is consistent with the peak formation of the SSE signal from YIG. Detailed analysis including polarization correction and Eckold-Sobolev-type resolution convolution, are now underway.

[1] C. Kittel, Phys. Rev. 110, 836 (1958).

[2] T. Kikkawa, K. Shen, B. Flebus, R. A. Duine, K. Uchida, Z. Qiu, G. E. W. Bauer, and E. Saitoh, Phys. Rev. Lett. 117, 207203 (2016).

[3] L. J. Cornelissen, K. Oyanagi, T. Kikkawa, Z. Qiu, T. Kuschel, G. E. W. Bauer, B. J. van Wees, and E. Saitoh, Phys. Rev. B 96, 104441 (2017).

[4] Y. Nambu, J. Barker, Y. Okino, T. Kikkawa, Y. Shiomi, M. Enderle, T. Weber, B. Winn, M. Graves-Brook, J. M. Tranquada, T. Ziman, M. Fujita, G. E. W. Bauer, E. Saitoh, and K. Kakurai, Phys. Rev. Lett.

in press.

Electric field effect on the magnon dispersion in α-$Cu_2V_2O_7$

Pharit Piyawongwatthana[A], Yano Shinichiro[B], Daisuke Okuyama[A], Kazuhiro Nawa[A], Kittiwit Matan[C], and Taku J Sato[A]
[A]*IMRAM, Tohoku University,* [B]*Mahidol University,* [C]*NSRRC*

The recent inelastic neutron scattering study on the noncentrosymmetric antiferromagnet α-$Cu_2V_2O_7$ revealed unusual magnon band splitting resulting from symmetry breaking [1]. The magnon band splitting splitting is due to the Dzyaloshinskii-Moriya (DM) interaction, and introduces the difference in the phase velocity of the counterrotating modes. For linearly polarized magnons, the difference of the phase velocity results in the rotation of the polarization direction. This effect is analogous to the optical rotation in noncentrosymmetric medias and may be used in future spintronics device.

Under the application of external electric field (E) in insulating polar compounds, the cations and anions may be moved in opposite directions. This way, the DM interaction may be enhanced through the strengthened symmetry breaking. This would lead to the putative electric-field-induced magnonic Faraday effect [2]. Therefore, in this experiment, we study the effect of E on the magnon dispersion of α-$Cu_2V_2O_7$ at SIKA in Australian Nuclear Science and Technology Organization.

In the experiment, we applied E along the crystallographic a- and c-axis of α-$Cu_2V_2O_7$. The figure shows the magnon dispersion of α-$Cu_2V_2O_7$ around 020 reflection (a) under zero E and (b) $E \sim 14.3$ kV/cm along the crystallographic c-axis, at the base temperature ($\sim$ 3K) collected with fixed final energy at 5 meV. We could not observe the change in the magnon dispersion due to E. For the application of E along the crystallographic a-axis, we were unable to confirm the change of the dispersion due to electrical discharge.

[1] G. Gitgeatpong, et al, Phys. Rev. Lett. 119, 047201 (2017)

[2] R. Cheng, et al, Sci. Rep. 6, 24223 (2016)

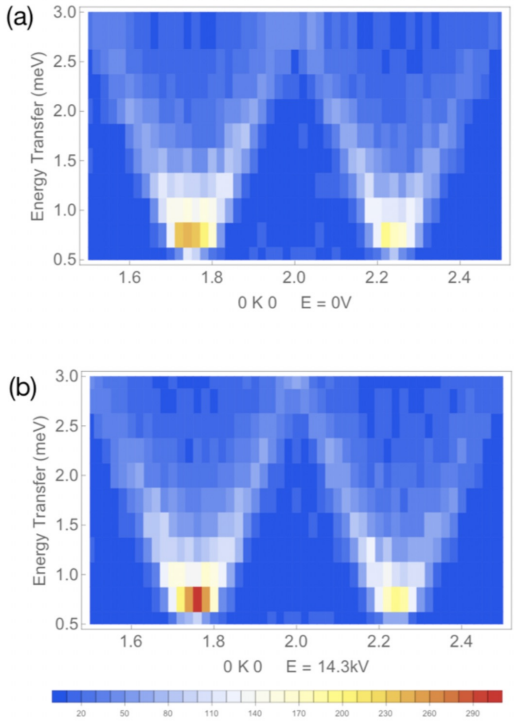

Fig. 1. Magnon dispersion of α-$Cu_2V_2O_7$ around 020 reflection under (a) zero E and (b) $E \sim 14.3$ kV/cm applied along crystallographic c-axis.

Strongly Correlated Electron System

Study of 2D Heavy Fermion Compounds $Ce(Te_{1-x}Se_x)_3$

R. Kobayashi[A], D. Ueta[B]
[A]*Univ. of the Ryukyus,* [B]*OIST*

Orthorhombic $CeTe_3$-type (space group $C2cm$) $CeTe_3$ may be the best sample to study 2D quantum critical phenomena in heavy fermion system. Rare-earth tritelluride $CeTe_3$, which belongs to the family of quasi-2D compounds RTe3 (where R = Y, La-Sm, Gd-Tm), has highly 2D crystal structure; RTe-slabs and two square Te-sheets are stacked along the b-axis[1,2]. RTe-slabs contribute to magnetism[1,3] and square Te-sheets induce 2D conducting bands, which give strongly anisotropic transport properties[2]. First-principles band-structure calculations revealed that the Fermi surface consists of inner and outer square sheets, large regions of which are nested by a single incommensurate wave-vector corresponding to the observed lattice-modulation[4,5]. Because of the characteristic quasi-2D nature of the Te sheet, the charge density wave (CDW) is formed with an extremely large gap of the order of 100 meV [6-9]. Bulk measurement studies using specific heat, electrical resistivity, and magnetic susceptibility clarified that $CeTe_3$ show successive antiferromagnetic(AFM) transition at T_{N1} = 3.1 K and T_{N2} = 1.3 K with electrical specific heat coefficient $\gamma = 0.9\ \mathrm{J/molK^2}$, which indicates that $CeTe_3$ forms heavy quasi-particles at low temperature although the ground state is still AFM order[10]. Very recently, our group has succeeded in growing single crystals of $Ce(Te_{1-x}Se_x)_3$ system and has studied x dependence of physical properties. T_{N1} and T_{N2} decrease with the increase of x and both disappear around x = 0.1. In addition, the γ value increases with the increase of x. These results indicate that the chemical pressure effect coming from Se substitution suppresses magnetic order and enhances Kondo effect due to the increase of c-f hybridization. The x = 0.1 sample may realize 2D quantum criticality at low temperature. Despite the extensive studies, there is no information about magnetic structure of $CeTe_3$ and its Se-substitution system. The determination of magnetic structure is necessary to understand 2D quantum criticality in the system. Additionally, the relation between CDW and AFM transition is also important to unveil how fermiology connects magnetism in the system. Therefore, the aim of this proposal is to determine magnetic structures in two different AFM phase (L-phase: $T < T_{N2}$, I-phase: $T_{N2} < T < T_{N1}$) and clarify how these AFM transition affect CDW phase. We also expect to detect diffuse scattering parallel to b-axis. The anomaly at T_{N1} in the specific heat measurements looks very broad, which implies the existence of 2D-like AFM order in I-phase.

Neutron scattering is suitable to study the structure of both CDW and AFM order in the same reciprocal lattice unit. Previous electron and neutron studies implied the existence of the nuclear propagation vector $k_0 = (0.71, 0, 0)$ and two different magnetic propagation vectors; one is $k_1 = (0.5, 0, 0.4)$, the other one is $k_2 = (0.18, 0, 0.68)$ [11]. However, observed magnetic peaks were not many. It is difficult to determine these magnetic structures from these peaks only.

In this experiment, we focused on $CeTe_3$ single crystal samples because of the machine time limitation. We have performed the experiments using the WOMBAT diffractometer at the OPAL reactor in ANSTO. The experiments used thermal neutron with a 1.54 Å and 2.95 Å wavelengths, which were monochromatized by a vertically focusing Ge-115 monochromator. The scattering planes of $CeTe_3$ single crystals were set on the $h0l$ scattering plane, where magnetic peaks were ob-

served in a previous study[11]. A dilution refrigerator was used to cool the samples, and the measurements were made in the temperature range of 50 mK 8.5 K.

Figure 1 shows the contour map of nuclear Bragg intensity in the h0l scattering plane at T = 8.5 K. All the observed nuclear scattering peaks can be explained by the space group of *Cmcm* and the lattice parameter of $CeTe_3$ consistently. Additionally, satellite nuclear peaks associated with the CDW order were also observed at the locations reported by ARPES measurements, which are in good agreement with the results of previous studies. Figure 2 (a,b,c,d) show contour plots of the Bragg scattering at 50 mK, and 1.5 K. Figure 2 (e,f) shows One-dimensional plots of the contour map integrated into Q direction. In the previous study, magnetic scattering peaks were observed in the region indicated by the blue dotted square in figure 2 (a,b). In the present study, however, no magnetic scattering peak was observed in this region. On the other hand, a ring-shaped weak Bragg scattering signal was observed in the low-Q region, as shown in figure 2 (c,d,e,f). This ring-shaped anomaly disappears above the antiferromagnetic transition temperature. Therefore, it is unlikely to be caused by polycrystalline impurities. We are planning to perform a follow-up experiment to investigate this ring-shaped anomaly with another spectrometer in the future.

[1] Y. Iyeiri, T. Okumura, C. Michioka, and K. Suzuki, Phys. Rev. B 67 144417 (2003).

[2] N. Ru and I. R. Fisher, Phys. Rev. B 73 033101 (2006).

[3] H. Chudo, C. Michioka, Y. Itoh, and K. Yoshimura, Phys. Rev. B 75 045113 (2007)

[4] J. Laverock, S. B. Dugdal, Z. Major, M. A. Alam, N. Ru, I. R. Fisher, G. Santi, and E. Bruno, Phys. Rev. B 71 085114 (2005)

[5] H. Yao, J. A. Robertson, E. A. Kim, and S. A. Kivelson, Phys. Rev. B 74 245126 (2006)

[6] V. Brouet, W. L. Yang, X. J. Zhou, Z. Hussain,N. Ru, K. Y. Shin, I. R. Fisher, and Z. X. Shen, Phys.Rev.Lett. 93 126405 (2004)

[7] H. Komoda, T. Sato, S. Souma, T. Takahashi, Y. Ito, and K. Suzuki, Phys. Rev. B 70 195101 (2004)

[8] C. Malliakas, S. J. L. Billinge, H. J. Kim, and M. G. Kanatzidis, J. Am. Chem. Soc. 127 6510 (2005)

[9] V. Brouet, W. L. Yang, X. J. Zhou, Z. Hussain, R. G. Moore, R. He, D. H. Lu, Z. X. Shen, J. Laverock, S. B. Dugdale, N. Ru, and I. R. Fisher, Phys. Rev. B 77 235104 (2008)

[10] K. Deguchi, T. Okada, G. F. Chen, S. Ban, N. Aso, and N. K. Sato, J. Phys.: Conf. Ser. 150 042023 (2009)

[11] K. Deguchi, Private communication

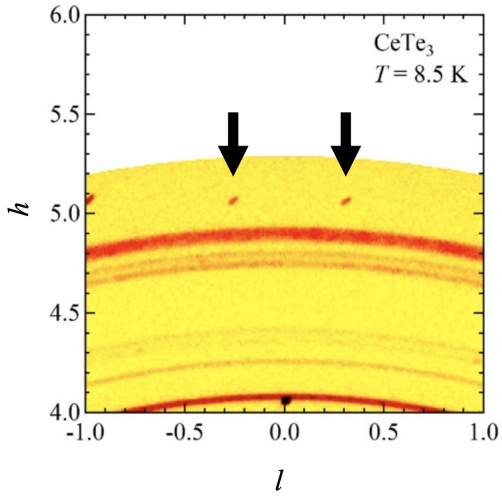

Fig. 1. Contour plot of the nuclear Bragg intensity in the (h, 0, l) scattering plane at T = 8.5 K. The black arrows indicate the satellite peaks coming from CDW order. These results are in good agreement with the results of the ARPES measurements.

Glasses and Liquids

Dynamics of super-high entropy liquids alkylated perfluorobenzenes

O. Yamamuro[A], M. Nirei[A], H. Akiba[A], T. Nakanishi[B], M. Tyagi[C], M. Wolf[D]
[A]ISSP-NSL, Univ. of Tokyo, [B]Kyoto Univ., [C]NCNR, NIST , [D]FRM II, TUM

The fusion (melting) temperature T_{fus} of molecules usually depend on molecular mass M; the larger M is, the higher T_{fus} becomes. For example, T_{fus} of benzene (C_6H_6, M = 78) is 279 K while that of biphenyl (C_6H_5-C_6H_5, M = 154) is 342 K. This is because the intermolecular van der Waals interaction is larger in the crystalline phase with denser molecular packing than that in the liquid phase with coarser packing. Recently, Nakanishi group in NIMS found that large molecules, 2,5-C_6C_{10}-tetraphenylporphyrin (2,5-C_6C_{10}-TPP) [1] and C_8C_{12}-perfluoro-benzene (C_8C_{12}-PFB), exist in liquid states at room temperature. It is quite interesting that T_{fus} of these alkylated molecules (2,5-C_6C_{10}-TPP, M = 2538; C_8C_{12}-PFB, M = 465) is lower than T_{fus} of non-alkylated molecules (TPP, M = 615, T_{fus} = 723 K; PFB, M = 186, T_{fus} = 278 K). We consider that these alkylated molecules are stabilized by the large entropy effect which is caused by the conformational disorder of long alkylchains. This situation is similar to that of ionic liquids which are in liquid states in spite of their strong interionic interactions. We collectively call this type of liquids "super-high entropy liquids (SHEL)".

In the present experiments, we have measured quasielastic neutron scattering (QENS) of alkylated perfluorobenzenes (APFB). These molecules are much smaller and simpler than alkylated TPP (ATPP), whose QENS have already been measured by us. The purpose of this work is to investigate the common dynamical features in APFB and ATPP. We take C_4C_8-PFB, C_6C_{10}-PFB and C_8C_{12}-PFB also to investigate the effect of the length of alkylchains.

Two QENS spectrometers, HFBS at NIST and TOFTOF at FRM II were used. They have different energy resolutions and can measure motions in different time regions (HFBS: 100 ps -10 ns, TOFTOF: 0.5 ps - 100 ps). To observe temperature dependence of motion, QENS have been measured at 4 or 5 temperature points above the glass transition temperature of each sample. $S(Q,\omega)$ data obtained by HFBS and TOFTOF were Fourier transformed to $I(Q,t)$ and then connected. $I(Q,t)$ curves were fitted to the two KWW functions corresponding to the relaxations of alkyl chains and the α-relaxations.

Figure 1 shows temperature dependence of $I(Q,t)$ curves of C_4C_8-PFB at Q = 1.0 Å^{-1} and fitting curves by two KWW functions. The fittings were satisfactory for all temperatures. The relaxation time of the α-relaxation tends to diverge at T_g, while that of alkyl chains is linear and independent of the α-relaxation. These results of APFB are quite similar to those of ATPP.

[1] A. Ghosh et al., Nat. Commun. 10, 4210 (2019).

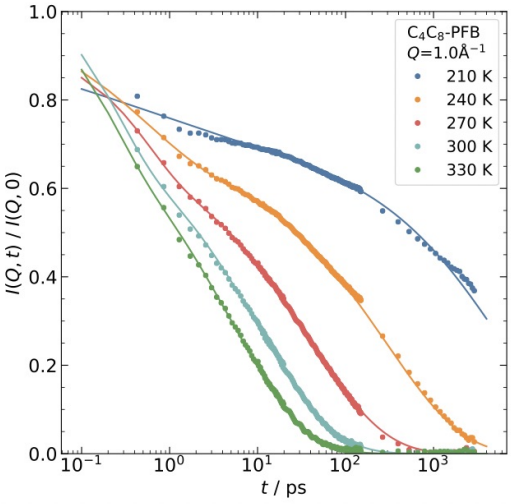

Fig. 1. Temperature dependence of $I(Q,t)$ of C_4C_8-PFB at Q = 1.0 Å^{-1} (circle) and fitting curves by two KWW functions (solid line).

Biology

Visualization of domain motion of tri-ubiquitin through segment deuteration and small-angle neutron scattering

Rintaro Inoue and Masaaki Sugiyama
Institute for Integrated Radiation and Nuclear Science, Kyoto University

It is well recognized that domain motions in multi-domain proteins play crucial roles in essential processes such as cellular signaling and gene regulation. Therefore, identification of their domain motions must be significant for revealing the mechanism to develop functions.

Ubiquitin (Ub) is a small protein comprised of 76 amino acid residues and is deeply related to regulatory roles in various cellular events such as cell cycle progression, DNA repair, transcriptional regulation, apoptosis and so on. The C-terminal group of Ub can be linked to another Ub through seven lysine (K) residues as well as the N-terminal amino groups, producing various types of poly-Ubs. We especially focused on linear K48 poly-Ub, which are expected to have high degree of freedom of constituting domains. As the first step, we started to study the structure and dynamics of linear K48-tri-ubiqutin (linear K48-tri-Ub). Solution NMR studies supposed that linear K48-tri-Ub could have four possible different states. Additional experimental approaches are indispensable for validating the expectation from NMR studies. Elucidation of relative spatial arrangements of two domains in linear K48-tri-Ub is one of the candidates for above-mentioned experimental requirements.Through the usage of ubiquitin-conjugating enzymes and deuteration of a domain, selective deuteration of concerned domain in linear K48-tri-Ubis is technically possible. We then prepared K48-tri-Ub consisted of two hydrogenated domains and 75% deuterated domain at different positions (H-H-75D). And we performed performed small-angle neutron scattering (SANS) measurement on H-H-75D in 100% D2O at 42 C, using Quokka installed at ANSTO. Figure 5 shows the SANS profiles from H-H-75D (red circle) and H-H-H (black circle). Clear difference of scattering profiles was observed between them, supporting the successful introduction of 75% deuterated domain into linear K48-tri-Ub. Aiming at the detailed structural analysis, we are on the progress of performing long time all- atom MD simulation.

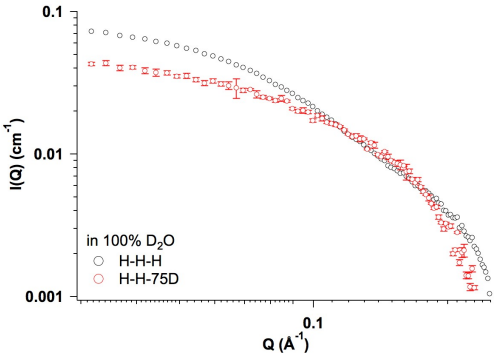

Fig. 1. SANS profiles from H-H-H and H-H-75D in 100% D2O at 42 C.

Soft Matters

Effect of a model scramblase peptide on viscoelastic properties of phspholipid bilayers

Hiroyuki Nakao
Faculty of Pharmaceutical Sciences, University of Toyama

Biological membranes consist mainly of phospholipids and proteins. During cellular processes, the morphology of lipid membranes changes dynamically, which is governed by interactions between lipids and proteins. Binding of cytosolic proteins to the membrane is often accompanied by the membrane deformation, such as invagination and tubulation. Many theoretical studies suggest that viscoelastic properties of the membrane play an important role in the membrane deformation. Some of the viscoelastic parameters can be determined by measuring the thermal fluctuations of the membrane, i.e., bending and thickness fluctuations, using neutron spin echo (NSE) spectroscopy.

Several studies suggested that lipid transbilayer movement (flip-flop) promoting peptides and proteins are involved in membrane deformation. We have previously developed a model "scramblase" peptide, TMP23Q, which has a glutamine residue in the center of the hydrophobic sequence and promotes phospholipid flip-flop. The specific aim of the present study is thus to evaluate how the presence of TMP23Q changes the thermal fluctuation and viscoelastic properties of the lipid membrane using NSE spectroscopy.

Thickness fluctuation measurement requires both tail-deuterated lipids, which are available only for saturated lipids. 1,2-Dimyristoyl-sn-glycero-3-phosphocholine (DMPC) has the most similar property in saturated lipids to that of biological membranes at 37 $^{\circ}$C. Therefore, we use a lipid mixture of DMPC and 1,2-dimyristoyl-sn-glycero-3-phosphoglycerol (DMPG) at a 95:5 molar ratio for bending fluctuation measurements, and a lipid mixture of 1,2-dimyristoyl-d54-sn-glycero-3-phosphocholine, DMPC, and DMPG at a 90:5:5 molar ratio for thickness fluctuation measurements. Here, 5% DMPG is included to prevent the formation of multilamellar vesicles. We prepared DMPC/DMPG vesicles containing TMP23Q or a negative control peptide TMP23L in D2O.

Intermediate scattering function obtained by bending fluctuation measurement was fit to a single-membrane fluctuation model proposed by Zilman and Granek with including the effect of internal dissipation within the bilayer proposed by Watson and Brown. The intrinsic bending modulus values were changed by the presence of neither peptides. The relaxation rate obtained from thickness fluctuation measurement at q ~ 1.0 nm $^{-1}$ showed discrepancy from Zilman-Granek theory (Fig. 1). Although we calculated the area compressibility modulus K_A, peptide inclusion in the membrane did not have any effect on K_A values. However, both peptides increased the relaxation time due to the thickness fluctuation τ_TF. Considering the relationship between the membrane viscosity and τ_TF, these results suggests that the presence of transmembrane peptides in the membrane increase the membrane viscosity.

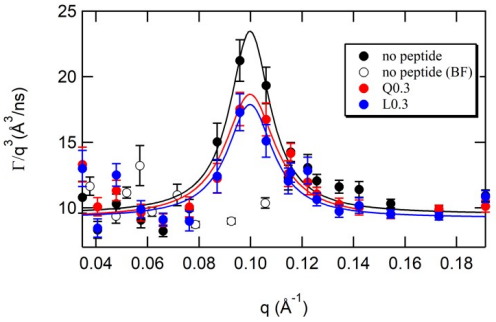

Fig. 1. Normalized relaxation rate Γ/q3 for tail-deuterated DMPC vesicles with/without peptides.